Spacelike matching to null infinity

Anıl Zenginoğlu, Manuel Tiglio

Department of Physics, and Center for Scientific Computation and Mathematical Modeling,
University of Maryland, College Park, MD 20742, USA

We present two methods to include the asymptotic domain of a background spacetime in null directions for numerical solutions of evolution equations so that both the radiation extraction problem and the outer boundary problem are solved. The first method is based on the geometric conformal approach, the second is a coordinate based approach. We apply these methods to the case of a massless scalar wave equation on a Kerr spacetime. Our methods are designed to allow existing codes to reach the radiative zone by including future null infinity in the computational domain with minor modifications. We demonstrate the flexibility of the methods by considering both Boyer-Lindquist and ingoing Kerr coordinates near the black hole. We also confirm numerically predictions concerning tail decay rates for scalar fields at null infinity in Kerr spacetime due to Hod for the first time.

I. INTRODUCTION

In numerical calculations of radiative fields, it is common to artificially truncate the computational domain by introducing an outer boundary into the spacetime. It is well known that this practice introduces conceptual and operational problems, specifically the outer boundary and the radiation extraction problems. [1, 2, 3, 4, 5, 6, 7, 8, 9, 10, 11, 12, 13, 14, 15, 16]. Each incremental development has taken considerably more effort, while a clean solution to the problems are available on a geometrical level, namely including the asymptotic domain on the computational grid [17, 18, 19, 20, 21, 22, 23].

First attempts on including the asymptotic domain on the numerical level have been based on using a compactifying coordinate along outgoing null surfaces [24, 25]. This allows one to include null infinity in the computational domain where no boundary conditions are required and radiation is naturally and unambiguously measured by idealized observers. In addition, the numerical evolution is very efficient as the grid follows outgoing radiation. Setting the numerical outer boundary to null infinity solves the aforementioned problems in a numerically efficient manner.

Unfortunately null foliations can be inconvenient, especially because they tend to develop caustics in dynamical spacetimes [26]. For solving the outer boundary and radiation extraction problems, however, we only need access to null infinity, whereas the interior foliation can be chosen arbitrarily. This observation suggests that one could match an arbitrary spacelike slice in the interior to an asymptotic domain that extends to null infinity. This has first been tried using Cauchy-characteristic matching [25, 27, 28, 29]. There, one uses an evolution based on Cauchy-type foliations in the interior and communicates the in- and outgoing characteristic variables along a timelike surface with a characteristic evolution in the asymptotic domain. This method introduces numerical difficulties due to the presence of a non-smooth matching along which the causal nature of the slicing changes from spacelike to null. While Cauchy-characteristic matching is a promising approach that requires further study, in this article we will explore an alternative approach to the problem.

Instead of matching spacelike slices to null slices along a timelike surface, here we use everywhere spacelike slices that approach null infinity in the asymptotic domain. The latter are called hyperboloidal surfaces as their behavior is similar to the standard hyperboloids in Minkowski spacetime [17]. They are more flexible than null surfaces because the only local condition restricting their choice is that they are spacelike. The asymptotic condition that they approach null infinity does not restrict the type of spacelike surfaces in the interior. It is favourable for numerical applications within the hyperboloidal approach that a gauge is chosen in which the location of future null infinity (scri) is independent of time, i.e. scri-fixing [30, 31, 32, 33, 34, 35]. Numerical experiments with scri-fixing have already been made successfully in spherically symmetric spacetimes [36, 37, 38, 39, 40, 41].

In this article we discuss the case of a fixed Kerr black hole background from the point of view of the hyperboloidal approach with scri-fixing. One might think that the characteristic approach should be sufficient for calculating radiative fields at null infinity when a background has been given. Indeed, for given Minkowski and Schwarzschild backgrounds, null coordinates are very useful and have been regularly applied in numerical calculations [25, 42, 43, 44]. In Kerr spacetime, however, they are difficult to deal with. There has been an ongoing effort to find a metric representing the Kerr geometry in Bondi-Sachs form that can be used in numerical computations [25, 45, 46, 47, 48], but to our knowledge no numerical calculations including null infinity could be presented so far.

The difficulties with the characteristic approach in Kerr spacetime arise, in part, from the fact that null coordinates are very rigid, i.e. the coordinate freedom for choosing a null surface is more restricted than for a spacelike surface.

The flexibility of hyperboloidal surfaces, on the other hand, allows us to evolve radiative fields on a Kerr spacetime up to and including null infinity while keeping, for example, standard Boyer-Lindquist or ingoing Kerr coordinates near the black hole [71]. We have chosen these foliations as they are the most common ones and have a different qualitative behaviour near the horizon. In principle, any foliation near the black hole can be chosen. The construction of such hyperboloidal surfaces in Kerr spacetime is relatively new [30]. In this article we show that it is also amenable to numerical calculations.

We discuss two methods for the numerical implementation of the hyperboloidal matching idea on the example of a scalar wave equation. In both methods matching includes certain choices of rescaling, time transformation and coordinate compactification. The first method is the well-known conformal method as introduced by Penrose [18, 19]. It requires knowledge of the conformal transformation behavior of the equation one is trying to solve. The second method is an essentially equivalent method that may be more appealing to researchers unfamiliar with conformal techniques. It considers the equation to be given in a certain coordinate system and applies the abovementioned transformations [36]. These methods allow us to solve the equations of interest including null infinity and can be applied within the hyperboloidal approach independent of matching.

We test our implementations by reproducing previously obtained quasi-normal mode frequencies [49, 50] and tail decay rates [51, 52, 53]. Our numerical tests focus on scalar fields but our method of including null infinity can be used with a wide variety of systems of evolution equations on a Kerr, Schwarzschild or Minkowski background that admit asymptotically flat solutions. In particular, the application of our techniques to calculate other types of radiative fields such as gravitational perturbations should be straightforward.

The article is organized as follows. In section II we present the main idea of hyperboloidal matching that allows us to include null infinity in the computational domain while using standard coordinates near the black hole. Section III presents the conformal method and applies it using ingoing Kerr coordinates, section IV presents the coordinate based method applied to Boyer-Lindquist coordinates. The resulting equations are then solved in section V using standard numerical techniques. Beyond confirming well-known predictions with our code, we also study decay rates for scalar perturbations of a Kerr black hole near and at null infinity confirming predictions due to Hod [54] for the first time. We conclude with a short discussion of our results.

II.   THE MAIN IDEA

As mentioned in the introduction, the construction of null coordinates in a Kerr background is relatively complicated [45, 46, 47, 48] whereas hyperboloidal foliations that are useful for numerical purposes can be given explicitly [30]. Following [30], we construct hyperboloidal foliations that coincide in an interior domain exactly with ingoing Kerr or Boyer-Lindquist coordinates.

The ingoing Kerr and Boyer-Lindquist representations of the Kerr metric will be given in terms of coordinates that we denote by (t, r, y, φ). Here, t is the time coordinate of the corresponding metric, r is a radial coordinate along level sets of t and y is an angular coordinate defined by $\cos \vartheta$ where ϑ and φ are the angular coordinates on a sphere. In order to match a spacelike surface to null infinity in a stationary spacetime, we introduce a new time coordinate τ of the form

$$\tau = t - h(r). \tag{1}$$

The function $h(r)$ is called the height function. The advantage of the above transformation is that it keeps the time direction invariant. The stationary Killing field that is timelike outside the event horizon has the same coordinate representation in both t and τ for any choice of $h(r)$. It is given by ∂_t or, equivalently, by ∂_τ. This implies that the Kerr metric in the new coordinates is manifestly stationary and natural observers that follow integral curves of the stationary Killing field are again given by surfaces of constant spatial coordinates. A natural consequence of the choice (1) is that null infinity is at a fixed spatial coordinate location with respect to a time-independent compactifying coordinate along level sets of τ. This considerably simplifies the numerical implementation as well as the analysis of the solution [31, 37].

A compactifying coordinate can be introduced by

$$r = \frac{\rho}{\Omega}, \qquad \text{with} \quad \Omega = \Omega(\rho). \tag{2}$$

This choice implies that the zero set of Ω corresponds to infinity in terms of the physical coordinate r. The choice of the conformal factor can be made in such a way as to ensure that future null infinity (denoted by $\mathscr{I}^+$) is at the coordinate location $\rho = S$, for example, by setting $\Omega_{\text{ext}}(\rho) = 1 - \rho/S$. In an interior domain near the black hole we want to use the standard physical coordinates, which implies $\Omega_{\text{int}}(\rho) = 1$. There is a transition between the interior

and the exterior domain where we match the two functions. Many choices are possible on the transition domain. Here we set

$$\Omega(\rho) = \begin{cases} \Omega_{\text{int}}(\rho) & \text{for} \quad \rho \leq \rho_{\text{int}}, \\ \Omega_{\text{int}}(\rho)\, e^{-(\rho-\rho_{\text{int}})^2/(\rho-\rho_{\text{ext}})^2} + \Omega_{\text{ext}}(\rho)\left(1 - e^{-(\rho-\rho_{\text{int}})^2/(\rho-\rho_{\text{ext}})^2}\right) & \text{for} \quad \rho_{\text{int}} < \rho < \rho_{\text{ext}}, \\ \Omega_{\text{ext}}(\rho) & \text{for} \quad \rho \geq \rho_{\text{ext}}. \end{cases} \tag{3}$$

Hyperboloidal foliations which coincide with standard Boyer-Lindquist or ingoing Kerr foliations in the interior can be constructed by suitably choosing the derivative of the height function, $dh/dr =: H$. Here we choose

$$H(\rho) = \begin{cases} 0 & \text{for} \quad \rho \leq \rho_{\text{int}}, \\ H_{\text{ext}}(\rho)\left(1 - e^{-(\rho-\rho_{\text{int}})^2/(\rho-\rho_{\text{ext}})^2}\right) & \text{for} \quad \rho_{\text{int}} < \rho < \rho_{\text{ext}}, \\ H_{\text{ext}}(\rho) & \text{for} \quad \rho \geq \rho_{\text{ext}}. \end{cases} \tag{4}$$

The choice $H = 0$ along with $\Omega = 1$ near the black hole ensures that the foliation and the coordinates are not changed. The function $H_{\text{ext}}(\rho)$ is different for Boyer-Lindquist and ingoing Kerr foliations [30]. Its choice will be discussed in later sections.

III.   THE CONFORMAL METHOD

The conformal method to study the asymptotic behaviour of radiative fields was introduced by Penrose [18, 19, 55]. The example of the scalar wave equation was the first system where the hyperboloidal initial value problem was studied [56, 57]. In this section we will present the conformal method for the scalar wave equation on a Kerr spacetime.

A.   Conformal transformation of the scalar wave equation

Our notation follows [37], where the conformal method was applied to calculate tail decay rates for scalar and Yang-Mills fields at null infinity in a Schwarzschild spacetime.

Here we are interested in solutions to the scalar wave equation $\tilde{\Box}\tilde{\phi} = 0$, for a scalar field $\tilde{\phi}$ in a Kerr spacetime with metric $\tilde{g}$. The coordinate transformations (1) and (2) result in a representation of the Kerr metric $\tilde{g}$ that is singular at $\Omega = 0$. To include null infinity in a regular way we need to rescale the Kerr metric $\tilde{g}$ with Ω^2. The Kerr spacetime is weakly asymptotically simple, implying that with a suitable choice of the transformations (1) and (2) the rescaled metric $g = \Omega^2\tilde{g}$ is smoothly extendable through null infinity where we have $\{\Omega = 0,\ d\Omega \neq 0\}$. The following conformal transformation rule holds

$$\left(\Box - \frac{1}{6}R\right)\phi = \Omega^{-3}\left(\tilde{\Box} - \frac{1}{6}\tilde{R}\right)\tilde{\phi}, \quad \text{with} \quad \phi = \frac{\tilde{\phi}}{\Omega}, \tag{5}$$

where R and $\tilde{R}$ are the Ricci scalars of the rescaled and the physical metrics g and $\tilde{g}$ respectively. The scalar wave equation with respect to the rescaled metric then becomes

$$\Box\phi - \frac{1}{6}R\phi = 0. \tag{6}$$

Note that the above equation is invariant under both coordinate and conformal transformations.

B.   First order reduction

The wave equation (6) can be written in any coordinate system $\{x^\mu\}$ as

$$g^{\mu\nu}\partial_\mu\partial_\nu\phi = \Gamma^\mu\partial_\mu\phi + \frac{1}{6}R\phi, \qquad \text{where} \qquad \Gamma^\lambda := g^{\mu\nu}\Gamma^\lambda_{\mu\nu}.$$

To bring it to first order form we introduce the auxiliary variables $\phi_\mu := \partial_\mu\phi$. Assuming that the coordinate x^0 denotes the time direction we get the following system of evolution equations

$$\begin{aligned} \left(-g^{00}\right)\partial_0\phi_0 &= 2g^{0a}\partial_a\phi_0 + g^{ab}\partial_a\phi_b - \left(\Gamma^0\phi_0 + \Gamma^a\phi_a + \frac{1}{6}R\phi\right), \\ \partial_0\phi_a &= \partial_a\phi_0, \\ \partial_0\phi &= \phi_0. \end{aligned} \tag{7}$$

The above system is symmetric hyperbolic [58]. Its coefficients are calculated with respect to the conformal metric g written in coordinates $\{\tau, \rho, y, \varphi\}$. In the case of a Kerr spacetime we can apply the separation of variables $\phi(\tau, \rho, y, \varphi) = \phi(\tau, \rho, y)e^{-i\,k\,\varphi}$ and study solutions for each k-mode independently, because azimuthal modes decouple in the presence of axisymmetry. Here we will choose initial data corresponding to a single azimuthal mode with $k = 0$. In this case, the indices a and b span over ρ and y.

C. Hyperboloidal compactification in ingoing Kerr coordinates

In the following, we present a hyperboloidal compactification of the ingoing Kerr representation of the Kerr metric. The ingoing Kerr slicing is one of the most commonly used slicing conditions for numerical calculations on Kerr spacetime. Its level sets allow us to apply an excision technique inside the black hole horizon. Asymptotically they approach spatial infinity. For their relation to the Boyer-Lindquist coordinates see [51]. Following usual notation we introduce

$$\widetilde{\Sigma} := r^2 + a^2 y^2, \qquad \widetilde{\triangle} := r^2 + a^2 - 2mr. \tag{8}$$

where m and a are the ADM-mass and the angular momentum of the Kerr spacetime, respectively. After transforming to compactifying coordinates we will use $\Sigma := \Omega^2 \widetilde{\Sigma}$ and $\triangle := \Omega^2 \widetilde{\triangle}$.

The Kerr metric in ingoing Kerr coordinates reads

$$
\tilde{g}_{\mathrm{iK}} = -\left(1 - \frac{2mr}{\widetilde{\Sigma}}\right) dt^2 + \frac{4mr}{\widetilde{\Sigma}} dt dr - \frac{4amr}{\widetilde{\Sigma}}(1 - y^2)\, dt\, d\varphi - 2a(1 - y^2)\left(1 + \frac{2mr}{\widetilde{\Sigma}}\right) dr d\varphi +
$$
$$
+ \left(1 + \frac{2mr}{\widetilde{\Sigma}}\right) dr^2 + \frac{\widetilde{\Sigma}}{1 - y^2} dy^2 + \left(r^2 + a^2 + \frac{2ma^2 r(1 - y^2)}{\widetilde{\Sigma}}\right)(1 - y^2)\, d\varphi^2 . \tag{9}
$$

This metric gives the following simple evolution equation for $\partial_t \tilde{\phi}_t$:

$$(\widetilde{\Sigma} + 2mr)\, \partial_t \tilde{\phi}_t = 4mr\, \partial_r \tilde{\phi}_t + \widetilde{\triangle}\, \partial_r \tilde{\phi}_r + (1 - y^2)\, \partial_y \tilde{\phi}_y + 2m\, \tilde{\phi}_t + 2(r - m)\, \tilde{\phi}_r - 2y\, \tilde{\phi}_y. \tag{10}$$

Applying the coordinate transformations (1) and (2) to the above metric and rescaling with Ω^2 gives

$$
g_{\mathrm{iK}} = -\Omega^2\left(1 - \frac{2m\rho\,\Omega}{\Sigma}\right) d\tau^2 - 2L\left(H - \frac{2m\rho\,\Omega}{\Sigma}(1 + H)\right) d\tau\, d\rho - \frac{4am\rho\,\Omega^3}{\Sigma}(1 - y^2)\, d\tau\, d\varphi + g_{\rho\rho}\, d\rho^2 -
$$
$$
- 2La(1 - y^2)\left(1 + \frac{2m\rho\Omega}{\Sigma}(1 + H)\right) d\rho d\varphi + \frac{\Sigma}{1 - y^2} dy^2 + \left(\rho^2 + a^2\Omega^2 + \frac{2ma^2\rho\Omega^3(1 - y^2)}{\Sigma}\right)(1 - y^2)d\varphi^2. \tag{11}
$$

Here, $L := \Omega - \rho\, \partial_\rho \Omega$, and

$$g_{\rho\rho} = \frac{L^2}{\Omega^2}\left(1 - H^2 + \frac{2m\rho\,\Omega}{\Sigma}(1 + H)^2\right).$$

The radial component of the spacetime metric appears to be singular, but with a suitable choice for the derivative of the height function it acquires an explicitly regular form. Following [30] we make that choice in the exterior domain to be

$$H_{\mathrm{ext}} = 1 + \frac{4m\Omega}{\rho} + \frac{(8m^2 - C_{\mathrm{iK}}^2)\Omega^2}{\rho^2}, \tag{12}$$

where C_{iK} is a free parameter. Only the first two terms are required for the regularity of $g_{\rho\rho}$. The third term (involving the free parameter C_{iK}) is taken for numerical purposes as will be discussed later. The appearance of such a free parameter for hyperboloidal foliations should be contrasted with asymptotic solutions to eikonal equations used for asymptotic constructions of null hypersurfaces, where no such parameters are allowed [47].

With the above choice for the derivative of the height function the metric is manifestly regular at $\mathscr{I}^+$. By setting $\Omega_{\mathrm{ext}} = 1 - \rho/S$ we get

$$g_{\mathrm{iK}}|_{\mathscr{I}^+} = -2\, d\tau\, d\rho + 2\,\frac{C_{\mathrm{iK}}^2}{S^2}\, d\rho^2 - 2a(1 - y^2)\, d\rho\, d\varphi + \frac{1}{1 - y^2}\, dy^2 + (1 - y^2)\, d\varphi^2.$$

The coordinate speed of outgoing characteristics at null infinity reads $c_+ = -2g_{\tau\rho}/g_{\rho\rho}$; for the above metric this is $c_+ = S^2/C_{\mathrm{iK}}^2$. We see that the coordinate speed of characteristics depends on the coordinate location of null infinity and an additional free parameter C_{iK}. The latter is related to the asymptotic value of the mean extrinsic curvature of our surfaces. This is the reason why we included the third term in the expansion (12): the parameter C_{iK} is important if we want the coordinate location of $\mathscr{I}^+$ to be large while avoiding strong restrictions on the allowed time step due to a large value of the coordinate speed of outgoing characteristics.

IV.   THE COORDINATE BASED APPROACH

We can recognize essentially three steps in the hyperboloidal compactification of Kerr spacetime: a time transformation (1), a spatial compactification (2), and a rescaling (5). In the previous section we calculated a conformal metric that has a smooth extension through null infinity and studied the conformal transformation behavior of the underlying covariant differential equation. In this section we will instead go through the above three steps at the level of the partial differential equations written in some coordinate system. We will follow this approach in an explicitly non-covariant notation. The rationale behind this is to have an alternative to the geometric approach which might be more straightforward to apply for those not familiar with conformal techniques. This approach may also be useful in cases where the conformal transformation behavior of the equation of interest is difficult to calculate [36].

A.   The transformations

Suppose that we are given a linear, second order partial differential equation for a function $\tilde{\phi}$ in two spatial dimensions,

$$\partial_t \tilde{\phi}_t = \tilde{A}^{tr} \partial_r \tilde{\phi}_t + \tilde{A}^{rr} \partial_r \tilde{\phi}_r + \tilde{A}^{yy} \partial_y \tilde{\phi}_y + \tilde{B}^t \tilde{\phi}_t + \tilde{B}^r \tilde{\phi}_r + \tilde{B}^y \tilde{\phi}_y + \tilde{C}\tilde{\phi}, \tag{13}$$

where $\tilde{\phi}_\mu := \partial_\mu \tilde{\phi}$. Assuming that the coefficients are independent of t, we write the above equation under the following transformations:

(i) Time transformation: We introduce a new time coordinate as in (1). Equation (13) then becomes

$$\begin{aligned}(1 - \tilde{A}^{rr} H^2 + \tilde{A}^{tr} H)\, \partial_\tau \tilde{\phi}_\tau &= (\tilde{A}^{tr} - 2H\tilde{A}^r)\partial_r \tilde{\phi}_\tau + \tilde{A}^{rr}\partial_r \tilde{\phi}_r + \tilde{A}^{yy}\partial_y \tilde{\phi}_y + \\ &+ (\tilde{B}^t - \tilde{B}^r H - \tilde{A}^{rr}\partial_r H)\tilde{\phi}_\tau + \tilde{B}^r \tilde{\phi}_r + \tilde{B}^y \tilde{\phi}_y + \tilde{C}\tilde{\phi},\end{aligned} \tag{14}$$

(ii) Spatial compactification: We introduce a compactifying radial coordinate as in (2). We set

$$J := \frac{d\rho}{dr} = \frac{\Omega^2}{L}, \qquad J' := \frac{dJ}{dr} = \frac{\Omega^3}{L^3}(2(\partial_\rho \Omega)L + \rho\,\Omega\partial_\rho^2\Omega),$$

with $L = \Omega - \rho\,\partial_\rho\Omega$ as before. Equation (13) becomes

$$\partial_t \tilde{\phi}_t = \tilde{A}^{tr} J\, \partial_\rho \tilde{\phi}_t + \tilde{A}^{rr} J^2\, \partial_\rho \tilde{\phi}_\rho + \tilde{A}^{yy}\partial_y \tilde{\phi}_y + \tilde{B}^t \tilde{\phi}_t + (\tilde{B}^r J + \tilde{A}^{rr} J')\,\tilde{\phi}_\rho + \tilde{B}^y \tilde{\phi}_y + \tilde{C}\tilde{\phi}. \tag{15}$$

(iii) Rescaling: We define the rescaled evolution variable $\phi := f(r)\tilde{\phi}$. Equation (13) becomes

$$\begin{aligned}\partial_t \phi_t &= \tilde{A}^{tr}\partial_r \phi_t + \tilde{A}^{rr}\partial_r \phi_r + \tilde{A}^{yy}\partial_y \phi_y + \left(\tilde{B}^t - \tilde{A}^{tr}\frac{\partial_r f}{f}\right)\phi_t + \left(\tilde{B}^r - 2\tilde{A}^{rr}\frac{\partial_r f}{f}\right)\phi_r + \tilde{B}^y \phi_y + \\ &+ \left(\tilde{C} - \tilde{B}^r \frac{\partial_r f}{f} + \tilde{A}^{rr}\left(2\frac{(\partial_r f)^2}{f^2} - \frac{\partial_r^2 f}{f}\right)\right)\phi\,.\end{aligned} \tag{16}$$

Combining the three steps above gives us finally an evolution equation of the form

$$\partial_\tau \phi_\tau = A^{\tau\rho}\partial_\rho \phi_\tau + A^{\rho\rho}\partial_\rho \phi_\rho + A^{yy}\partial_y \phi_y + B^\tau \phi_\tau + B^\rho \phi_\rho + B^y \phi_y + C\phi. \tag{17}$$

This method is essentially equivalent to the conformal method. Equation (7), which we obtained with the conformal method, can also be derived by using the coordinate based approach just presented and making consistent choices

of rescaling and coordinate transformations. This has been used as a check for the final equations that the have numerically implemented.

Note that in the coordinate based method we do not need to rescale the function $\tilde{\phi}$ with Ω. We can choose to rescale it with any function that behaves asymptotically like r, and read off the radiation field directly at null infinity. In fact, a common approach in numerical calculations is to evolve the variable $\phi := r\tilde{\phi}$. To see how this relates to the conformal rescaling of the previous section, make a simple choice for the conformal factor: $\Omega = 1 - \rho$. In terms of the physical coordinate r we have have

$$r = \frac{\rho}{1-\rho} \quad \Rightarrow \quad \rho = \frac{r}{1+r} \quad \Rightarrow \quad \Omega = 1 - \rho = \frac{1}{1+r}.$$

Therefore and due to the fall-off behavior of $\tilde{\phi}$, the rescaling $\tilde{\phi}/\Omega = (1+r)\tilde{\phi}$ is asymptotically equivalent to the rescaling $r\tilde{\phi}$.

B. Hyperboloidal compactification of the scalar wave equation in Boyer-Lindquist coordinates

We have used the above method to transform the scalar wave equation on a Kerr background written in Boyer-Lindquist coordinates. The Kerr metric in those coordinates reads

$$\tilde{g}_{\mathrm{BL}} = -\left(1 - \frac{2mr}{\widetilde{\Sigma}}\right) dt^2 - \frac{4amr}{\widetilde{\Sigma}}(1-y^2)\, dt\, d\varphi + \frac{\widetilde{\Sigma}}{\widetilde{\triangle}}\, dr^2 + \frac{\widetilde{\Sigma}}{1-y^2}\, dy^2 + \tilde{R}^2\left(1-y^2\right) d\varphi^2.$$

Instead of writing the conformal Kerr metric we derive the scalar wave equation on this background and work directly with that equation. It is common practice to introduce the tortoise coordinate r_* for the numerical implementation of the wave equation because the Boyer-Lindquist coordinates do not give a foliation of the event horizon. The tortoise coordinate is defined by

$$\frac{dr_*}{dr} = \frac{r^2 + a^2}{\widetilde{\triangle}}.$$

The scalar wave equation in Boyer-Lindquist coordinates can be written as

$$\begin{aligned}
\partial_t \tilde{\phi}_t &= \frac{(r^2+a^2)^2}{D^2}\partial_{r_*}\tilde{\phi}_{r_*} + \frac{\widetilde{\triangle}(1-y^2)}{D^2}\partial_y\tilde{\phi}_y + \frac{2r\widetilde{\triangle}}{D^2}\tilde{\phi}_{r_*} - \frac{2y\widetilde{\triangle}}{D^2}\tilde{\phi}_y, \\
\partial_t \tilde{\phi}_{r_*} &= \partial_{r_*}\tilde{\phi}_t, \qquad \partial_t\tilde{\phi}_y = \partial_y\tilde{\phi}_t, \qquad \partial_t\tilde{\phi} = \tilde{\phi}_t,
\end{aligned} \tag{18}$$

where we have defined $D^2 := (r^2+a^2)^2 - a^2\widetilde{\triangle}(1-y^2)$. From the above equation we calculate the equation for a rescaled variable $\phi := r\,\tilde{\phi}$ following the prescription given by equation (16). Then we introduce a time function τ as in equation (14), such that the level surfaces of τ approach null infinity. The Kerr metric in Boyer-Lindquist coordinates approaches a Schwarzschild metric in standard Schwarzschild coordinates, therefore we may assume that the asymptotic form of H needs to be chosen as for the Schwarzschild spacetime in standard Schwarzschild coordinates. Remember, however, that the asymptotic Schwarzschild metric in null directions in the tortoise coordinate is of standard Minkowski form. Therefore, we can choose for H the expression for the standard hyperboloids in Minkowski spacetime [30]. We set

$$H_{\mathrm{ext}} = \frac{r_*}{\sqrt{r_*^2 + C_{\mathrm{BL}}^2}} = \frac{\rho}{\sqrt{\rho + \Omega^2 C_{\mathrm{BL}}^2}}. \tag{19}$$

For the second part of the above equation we used $r_* = \rho/\Omega$. Here C_{BL} is a free parameter that determines the asymptotic extrinsic curvature of the hyperboloidal surfaces as in the case of Minkowski spacetime [30, 59]. As in the ingoing Kerr case, the value of C_{BL} needs to be chosen close to the value of the coordinate location of null infinity, S, in order to prevent the coordinate speeds of outgoing characteristics from becoming too large.

For the spatial compactification (2) we choose the function Ω as in the ingoing Kerr case. Notice that here Ω just determines the spatial coordinate compactification and does not acquire the meaning of a conformal factor for the spacetime metric.

The above choices fix the transformations and result in an explicitly regular set of equations each of which has the form (17). Their final form is rather lengthy but straightforward to calculate and will therefore not be presented.

V. NUMERICS

As a test of the two approaches to include null infinity in numerical simulations by spacelike matching 'standard' Cauchy hypersurfaces to hyperboloidal slicings here we implement them on a $2+1$ code solving a scalar wave equation on a Kerr spacetime. Near the black hole we use ingoing Kerr and Boyer-Lindquist coordinates.

The conformal method is applied for the hyperboloidal compactification in the ingoing Kerr case, and the coordinate based approach in the Boyer-Lindquist case. We note that there is no specific reason for this choice. Other coordinate choices are possible as well. The equations we solve numerically are given in Eq. (7) with respect to the metric (11) and in Eq. (18) with the transformations (14), (15), and (16). The asymptotic form of the height functions for ingoing Kerr and Boyer-Lindquist foliations are (12) and (19) respectively.

In both cases we prescribe initial data of the form

$$\phi(0, \rho, y) = 0, \qquad \phi_\tau(0, \rho, y) = e^{-(r-r_0)^2/\sigma^2} Y_{l0} \tag{20}$$

where Y_{l0} denotes the familiar spherical harmonics of degree l and order $m = 0$. The data is of compact support. We set $\phi_\tau(0, \rho, y) = 0$ for $\rho > \rho_{\text{int}}$. Regarding the parameters in the initial data we choose $r_0 = 5$ and $\sigma = 2$ with mass $m = 1$.

A. The numerical method

We use method of lines with fourth order Runge-Kutta time integration. For the angular derivatives we use a pseudospectral collocation method with Legendre polynomials, as in [53], which is both efficient and automatically takes care of the coordinate singularities at the poles. We use finite differences in the radial direction. The reason why we do not use spectral differencing in the radial direction is the non-smooth matching (3) and (4). We wish to remark, however, that we could, in principle, apply spectral differencing by using a multipatch approach in which the matching boundaries coincide with some of the patch boundaries. We did not follow this approach only due to the simplicity of the finite difference method.

In the ingoing Kerr case the inner boundary is a spacelike surface inside the event horizon so that one can use the excision technique. The outer boundary is at null infinity. We apply one-sided finite differencing at both boundaries using the same order operators at the boundaries as in the interior [60]. In the Boyer-Lindquist case we set the inner boundary very close to the black hole. We apply the outgoing boundary condition (ingoing with respect to the black hole) at the inner boundary, which we set at $r_* = -40m$. We use fourth order accurate finite differencing operators in the Boyer-Lindquist case instead of the eight order operators used in the ingoing Kerr case, as the outgoing boundary condition is simpler to apply with respect to fourth order operators.

We add Kreiss-Oliger type artificial dissipation to the evolution equation for the time derivative of ϕ to suppress numerical high-frequency waves [61]. For a $2p - 2$ accurate scheme we choose an operator (Q) of order $2p$ as

$$Q = \epsilon(-1)^p \frac{h^{2p-1}}{2^p} D_+^p D_-^p,$$

where h is the grid size, $D_\pm$ are the forward and backward finite differencing operators and ϵ is the dissipation parameter which we set as $\epsilon = 0.03$.

One major source of error is the matching between the inner coordinates and the coordinates of the hyperboloidal compactification. The matching is performed using Eqs. (3) and (4). We found that the matching along ρ_{int} introduces large numerical errors in the solution that converge with the order of the finite differencing method. The fact that the numerical errors are large near ρ_{int} is to be expected because the matching is not analytic at ρ_{int} whereas it is analytic at ρ_{ext}. In our simulations we set ρ_{int} to be at around $20m$ in both cases. This is a point where improvement may lead to a more efficient code. The outer matching introduces no problems.

We put the numerical outer boundary at $\rho = S = 100$ in both cases. The numerical outer boundary corresponds to future null infinity. Its coordinate location effects the coordinate speed of characteristics as discussed before. Experiments with different coordinate locations of future null infinity delivered qualitatively similar results. An important point with respect to the coordinate location of the outer boundary is related to the choice of parameters that determine the hyperboloidal foliation. The free parameters C_{iK} and C_{BL} need to be both of the order of S as discussed in III C and IV B.

The convergence properties of our codes can be seen in Figure 1. For these plots, a three level convergence analysis has been performed for an $l = 0$ initial data using 1600, 3200 and 6400 grid cells in the radial direction and 4 points in the angular direction where spectral differencing was applied. We used quadruple precision for the runs because the numerical error was below machine accuracy at late times when double precision was used. The time step for the
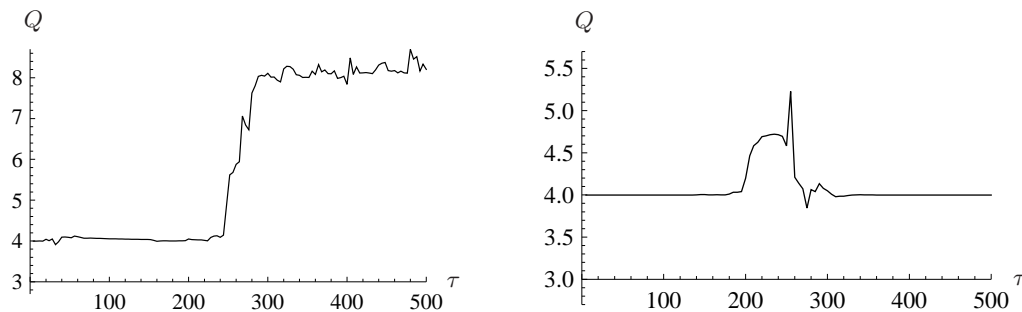
Figure 1: Convergence in the L2-norm in the radial direction for ingoing Kerr (left plot) and Boyer-Lindquist (right plot) coordinates near the black hole. The convergence factor Q is calculated by $Q = \log_2 \frac{\|\phi^{low} - \phi^{med}\|_{L_2}}{\|\phi^{med} - \phi^{high}\|_{L_2}}$ where the norm is taken over the whole grid at a given time. We see that in the ingoing Kerr case the convergence factor attains its value 8 after a transient phase because numerical errors in the time integration dominate as observed in [36]. In the Boyer-Lindquist case the convergence factor is 4. The irregularities in the convergence factors are due to matching.

ingoing Kerr case was $dt = 0.05$ while for the Boyer-Lindquist case it was $dt = 0.1$. The reason why we can choose a larger time step in the Boyer-Lindquist case is because the coordinate speeds of characteristics are lower.

We see that, in the ingoing Kerr case, the convergence factor settles down at around 8 after an initial transient phase in which it starts at 4, the order of the time integration. The reason is that in this initial phase the error is dominated by the time integration. This is the same behavior as in [36]. To get a convergence factor of 8 from the beginning a much lower time step needs to be chosen which is not practical for late-time tail calculations [36]. In the Boyer-Lindquist case where both the time integration and the spatial discretization is of fourth order the convergence factor is 4. The irregularities in the plots are due to matching. When a wave package passes through the matching boundary ρ_{int}, the error increases significantly but in a convergent fashion.
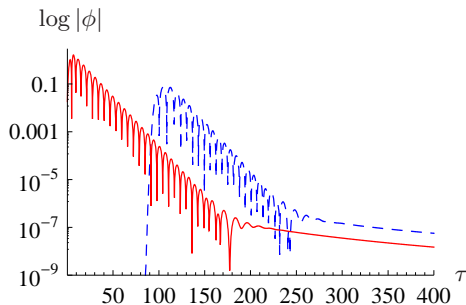

Figure 2: Quasi-normal mode ringing of Kerr spacetime with $m = 1$ and $a = 0.5$ excited by a Gaussian initial data with $l = 2$ mode as measured by an observer located along $r = 3m$ (the solid red curve) and $\mathscr{I}^+$ (the dashed blue curve) in ingoing Kerr coordinates.

As a next test we calculate a fundamental quasi-normal mode frequency. The quasi-normal mode ringing for initial data with $l = 2$ can be seen in Figure 2. We plot here the ringing as measured by an observer at $r = 3m$ and at $\mathscr{I}^+$ in ingoing Kerr coordinates. We observe that the duration of ringing along $\mathscr{I}^+$ is shorter. Therefore we use the signal measured closer to the black hole for the fitting. The frequencies are obtained by fitting the signal to the formula

$$\phi(\tau) = A \, e^{-\omega_2 \tau} \sin(\omega_1 \tau + \varphi). \tag{21}$$

Here, ω_1 and ω_2 are the mode frequencies, A is the amplitude and φ is the phase of the wave signal. The fitting is performed using a simple least squares method on the interval $\tau \in [60m, 150m]$. The error in frequency is rather dominated by the fit than by numerics. We find $\omega_1 = 0.491971$ and $\omega_2 = 0.094653$. These numerical values are very close to those obtained by using Leaver's continued fraction method [62, 63], which read $\omega_1 = 0.49196$ and $\omega_2 = 0.09463$. The latter have also been confirmed numerically by other codes [49, 50]. We obtain a similar result with the code based on Boyer-Lindquist coordinates.

Quasi-normal mode frequencies are the same for all observers. Including null infinity in the computational domain does not give us a different picture. The tail decay rates, however, vary from observer to observer as discussed in the next subsection.

B. Tail decay rates

In contrast to the quasinormal mode frequencies, the asymptotic tail decay rates at a finite distance and at null infinity are different. Also, before the asymptotic decay rates are obtained, the signals differ substantially from each other. The signal that is relevant for an idealized observer is the one measured at null infinity. This is because realistic sources of gravitational radiation are at astronomical distances from us. Our detectors are better modelled by observers at future null infinity than by observers at finite distances in numerical computations [37, 64, 65].
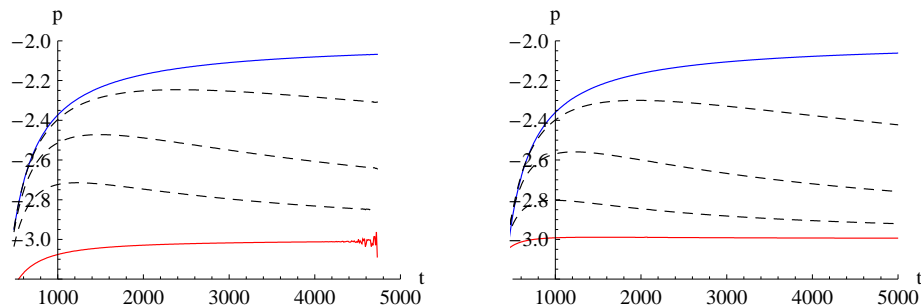

Figure 3: Tail decay rates for initial data with a pure $l = 0$ mode in ingoing Kerr (left) and Boyer-Lindquist (right) coordinates. The solid blue curves are measured by observers along $\mathscr{I}^+$. The solid red curves are measured by observers close to the black hole at $r = 10$ in units where mass $m = 1$. The dashed black curves correspond to observers at $r = \{5000, 1000, 500\}$ from top to bottom.

The transition between timelike and null infinity in the decay rates for a monopole perturbation can be seen in Figure 3. In that figure, the local power index has been plotted for various observers ordered by distance ranging from close to the black hole up to and including future null infinity. We define the local power index as

$$p_{\rho,y}(\tau) = \frac{d \ln |\phi(\tau, \rho, y)|}{d \ln \tau}. \tag{22}$$

We calculate the time derivatives by using finite differencing from numerical data. The function $p_{\rho,y}(\tau)$ becomes the exponent of the polynomial decay of the solution asymptotically in time. We did not observe a significant variation of the index with respect to the angular location y of the observer.
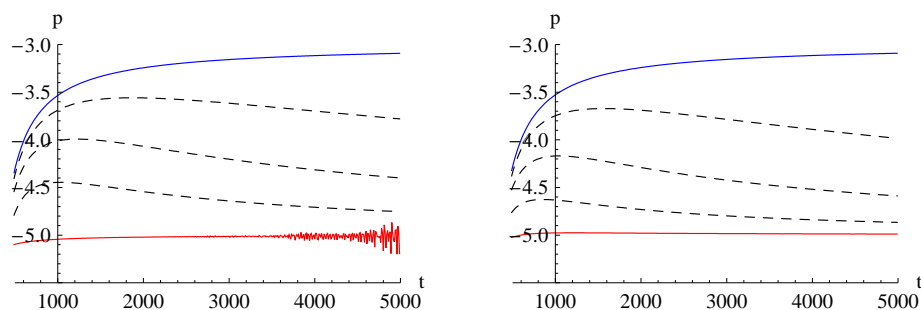

Figure 4: Tail decay rates for an $l = 1$ mode. Observers are located as in Figure 3.

We see that the monopole perturbation decays with rate -3 near timelike infinity, while the rate at null infinity is -2. The decay rate for the $l = 1$ mode is -5 near the black hole and -3 near null infinity, as can be seen in Figure 4. This behavior is the same as in Schwarzschild spacetime and is in accordance with the prediction of Table II in [54]. The decay rate for $l = 2$ is as for $l = 0$ and the rate for $l = 3$ is as for $l = 1$ due to mode coupling in accordance with earlier predictions and calculations [51, 52, 53, 54]. For the $l = 4$ mode the decay rate near timelike infinity is -5 but along null infinity it is -4. This is also in accordance with Hod's prediction (see Table I in [54]).

We see that the calculation in ingoing Kerr coordinates near the black hole is not as accurate as in Boyer-Lindquist coordinates. This is due to the smaller time step in the ingoing Kerr case as mentioned in Section V A.

We mention that from a physical point of view, in an axisymmetric spacetime the concept of a pure l-mode initial data does not have a geometrically invariant meaning. In this case, only the monopole perturbations can be defined invariantly. This has led to some confusion about decay rates for Kerr spacetime. In our studies the asymptotic decay

rates in both coordinate systems coincide for any l-mode initial data as in (20) due to the fact that we are using the same type of initial data in coordinates that are related in a way which leaves the notion of an l-mode invariant as explained in [51]. Here we found that the asymptotic rates are the same for such initial data in ingoing Kerr and Boyer-Lindquist coordinates also at null infinity.
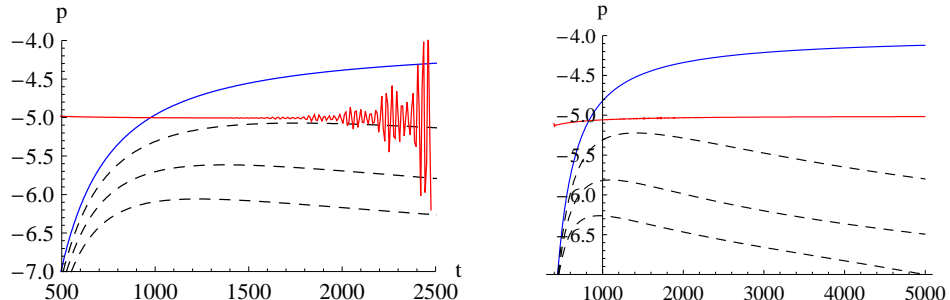

Figure 5: Tail decay rates for an $l = 4$ mode. Observers are located as in Figure 3.

VI. DISCUSSION

We have presented the first numerical evolution scheme for scalar fields on the background of a rotating black hole that includes future null infinity. Our method is based on the construction of hyperboloidal surfaces in Kerr spacetime presented in [30]. While previous studies of characteristic foliations do allow, in principle, compactification at null infinity on a Kerr spacetime [45, 46, 47, 48], they did not culminate in numerical applications. In this paper we have presented and implemented two methods based on the hyperboloidal compactification technique that include null infinity in the computational domain. Our methods are very flexible and allow us to keep any preferred choice of coordinates near the black hole.

We confirmed well-known results concerning quasi-normal mode frequencies and tail decay rates measured by observers close to the black hole. In addition, we presented decay rates at and near null infinity confirming earlier predictions [54] for the first time. Our method allows us to study the transition between timelike and null infinity with respect to the decaying signal.

We expect that our methods can be applied to discuss physically more interesting evolution equations so that predictions concerning the behaviour of electromagnetic and gravitational perturbations at future null infinity can be studied as well [66, 67]. The coordinate based approach of Section III may be easier to apply to problems where the conformal transformation behavior is not known. In numerical calculations the equations of interest are given anyway in a specific coordinate system. Once the asymptotic form of the height function is known, the coordinate based approach can be applied easily to transform the equations to include null infinity in the computational domain.

In numerical applications of the hyperboloidal approach, one usually finds that the hyperboloidal method is very efficient in calculating the outgoing radiation accurately [36, 37]. In our study of spacelike matching, however, we find that the presence of a matching domain is a significant source of numerical error. There are many possibilities to solve this problem. One option is to devise better matching techniques, such as matching at a multipatch boundary. This approach will still have to deal with the change of characteristic speeds across the matching domain. The other option would be to construct an analytic, horizon penetrating hyperboloidal foliation which renders the introduction of matching domains unnecessary. It would be interesting to study hyperboloidal foliations of Kerr spacetime analytically or numerically using methods that proved useful in the case of Schwarzschild spacetime [68, 69, 70].

This work suggests that once the spherically symmetric case has been mastered, extension to less symmetries is more or less straightforward in the hyperboloidal approach. There are two reasons for this. First, hyperboloidal foliations can be made to coincide with any known foliation near the black hole [30]. This allows us to use methods that have been applied successfully in numerical relativity in an inner domain where the fields are strong. Second, asymptotically flat spacetimes become flat, and therefore spherically symmetric in the asymptotic domain. As a consequence the spherically symmetric case already gives important clues on how to deal with the asymptotic region in the hyperboloidal approach.

The observations presented in this article may be useful in the fully nonlinear case, once the hyperboloidal evolution problem with the Einstein equations is solved. Specifically, the numerical discussion of having null infinity at an arbitrary but fixed spatial coordinate location and setting the conformal factor to unity in the interior while allowing it to vanish in the asymptotic domain in a certain way can be expected to be relevant in the nonlinear case.

Acknowledgments

This work was supported in part by the NSF grant PHY0801213 to the University of Maryland. We thank Frank Herrmann and Ted Jacobson for discussions.

[1] Olivier Sarbach and Manuel Tiglio. Boundary conditions for Einstein's field equations: Analytical and numerical analysis. *J. Hyperbol. Diff. Equat.*, 2:839, 2005.

[2] Oliver Rinne. Stable radiation-controlling boundary conditions for the generalized harmonic Einstein equations. *Class. Quant. Grav.*, 23:6275–6300, 2006.

[3] Helmut Friedrich. Initial boundary value problems for Einstein's field equations and geometric uniqueness. 2009.

[4] E. Deadman and J. M. Stewart. Numerical Relativity and Asymptotic Flatness. *Class. Quant. Grav.*, 26:065008, 2009.

[5] Emanuel Gallo, Luis Lehner, and Osvaldo Moreschi. Estimating total momentum at finite distances. *Phys. Rev.*, D78:084027, 2008.

[6] Oliver Rinne, Lee Lindblom, and Mark A. Scheel. Testing outer boundary treatments for the Einstein equations. *Class. Quant. Grav.*, 24:4053–4078, 2007.

[7] Enrique Pazos, Ernst Nils Dorband, Alessandro Nagar, Carlos Palenzuela, Erik Schnetter, and Manuel Tiglio. How far away is far enough for extracting numerical waveforms, and how much do they depend on the extraction method? *Class. Quantum Grav.*, 24:S341–S368, 2007.

[8] H. Friedrich and G. Nagy. The initial boundary value problem for Einstein's vacuum field equations. *Commun. Math. Phys.*, 201:619–655, 1999.

[9] Michael Boyle et al. High-accuracy comparison of numerical relativity simulations with post-Newtonian expansions. *Phys. Rev.*, D76:124038, 2007.

[10] Michael Boyle and Abdul H. Mroue. Extrapolating gravitational-wave data from numerical simulations. 2009.

[11] Lee Lindblom, Benjamin J. Owen, and Duncan A. Brown. Model Waveform Accuracy Standards for Gravitational Wave Data Analysis. *Phys. Rev.*, D78:124020, 2008.

[12] H. O. Kreiss, O. Reula, O. Sarbach, and J. Winicour. Boundary conditions for coupled quasilinear wave equations with application to isolated systems. 2009.

[13] Andrea Nerozzi and Oliver Elbracht. Using curvature invariants for wave extraction in numerical relativity. 2008.

[14] Luis Lehner and Osvaldo M. Moreschi. Dealing with delicate issues in waveforms calculations. *Phys. Rev.*, D76:124040, 2007.

[15] Luisa T. Buchman and Olivier C. A. Sarbach. Improved outer boundary conditions for Einstein's field equations. *Class. Quant. Grav.*, 24:S307–S326, 2007.

[16] A. M. Abrahams et al. Gravitational wave extraction and outer boundary conditions by perturbative matching. *Phys. Rev. Lett.*, 80:1812–1815, 1998.

[17] Helmut Friedrich. Cauchy problems for the conformal vacuum field equations in general relativity. *Comm. Math. Phys.*, 91:445–472, 1983.

[18] Roger Penrose. Asymptotic properties of fields and space-times. *Phys. Rev. Lett.*, 10:66–68, 1963.

[19] Roger Penrose. Gravitational collapse and space-time singularities. *Phys. Rev. Lett.*, 14:57, 1965.

[20] Louis A. Tamburino and Jeffrey H. Winicour. Gravitational Fields in Finite and Conformal Bondi Frames. *Phys. Rev.*, 150:1039–1053, 1966.

[21] Peter Hübner. Method for calculating the global structure of (singular) spactimes. *Phys. Rev. D*, 53:701–721, 1996.

[22] Sascha Husa. In L. Fernández and L. Manuel González, editors, *Proceedings of the 2001 Spanish Relativity meeting*, volume 617 of *Lecture Notes in Physics*, pages 159–192. Springer, 2003.

[23] Jorg Frauendiener. Conformal infinity. *Living Rev. Relativity*, 7(1), 2004. http://www.livingreviews.org/lrr-2004-1.

[24] R. A. Isaacson, J. S. Welling, and J. Winicour. Null cone computation of gravitational radiation. *J. Math. Phys.*, 24:1824–1834, 1983.

[25] Jeffrey Winicour. Characteristic Evolution and Matching. 2008.

[26] H. Friedrich and J. Stewart. Characteristic initial data and wave front singularities in general relativity. *Proc. R. Soc.*, A385:345–371, 1983.

[27] J. L. Anderson and D. W. Hobill. A study of nonlinear radiation damping by matching analytic and numerical solutions. *J. Comput. Phys.*, 75:283, 1988.

[28] Nigel T. Bishop. Numerical relativity: Combining the Cauchy and characteristic initial value problem. *Class. Quant. Grav.*, 10:333–341, 1993.

[29] Nigel T. Bishop, Roberto Gómez, Paulo R. Holvorcem, Richard A. Matzner, Philippos Papadopoulos, and Jeffrey Winicour. Cauchy-characteristic matching: A new approach to radiation boundary conditions. *Phys. Rev. Lett.*, 76(23):4303–4306, 3 June 1996.

[30] Anıl Zenginoğlu. Hyperboloidal foliations and scri-fixing. *Class. Quant. Grav.*, 25:145002, 2008.

[31] Sascha Husa, Carsten Schneemann, Tilman Vogel, and Anil Zenginoglu. Hyperboloidal data and evolution. *AIP Conf. Proc.*, 841:306–313, 2006.

[32] J. Frauendiener. Numerical treatment of the hyperboloidal initial value problem for the vacuum Einstein equations. II. the

evolution equations. *Phys. Rev. D*, 58:064003, 1998.

[33] Charles W. Misner. Over the Rainbow: Numerical Relativity beyond Scri+. 2005.

[34] Vincent Moncrief and Oliver Rinne. Regularity of the Einstein Equations at Future Null Infinity. *Class. Quant. Grav.*, 26:125010, 2009.

[35] Lars Andersson. Construction of hyperboloidal initial data. *Lect. Notes Phys.*, 604:183–194, 2002.

[36] Anıl Zenginoğlu, Darío Núñez, and Sascha Husa. Gravitational perturbations of Schwarzschild spacetime at null infinity and the hyperboloidal initial value problem. *Class. Quant. Grav.*, 26:035009, 2009.

[37] Anıl Zenginoğlu. A hyperboloidal study of tail decay rates for scalar and Yang-Mills fields. *Class. Quant. Grav.*, 25:175013, 2008.

[38] Gyula Fodor and István Rácz. What Does a Strongly Excited 't Hooft–Polyakov Magnetic Monopole Do? *Phys. Rev. Lett.*, 92(15):151801, 2004.

[39] Gyula Fodor and Istvan Racz. Numerical investigation of highly excited magnetic monopoles in SU(2) Yang-Mills-Higgs theory. *Phys. Rev.*, D77:025019, 2008.

[40] James R. van Meter, David R. Fiske, and Charles W. Misner. Excising das All: Evolving Maxwell waves beyond Scri. *Phys. Rev.*, D74:064003, 2006.

[41] Piotr Bizon and Anil Zenginoglu. Universality of global dynamics for the cubic wave equation, 2008.

[42] Manuela Campanelli, Roberto Gomez, Sascha Husa, Jeffrey Winicour, and Yosef Zlochower. The close limit from a null point of view: The advanced solution. *Phys. Rev. D*, 63:124013, 2001.

[43] C. Gundlach, R. Price, and J. Pullin. Late-time behaviour of stellar collapse and explosions: I. linearized perturbations. *Phys. Rev. D*, 49, 1994.

[44] Sascha Husa, Yosef Zlochower, Roberto Gomez, and Jeffrey Winicour. Retarded radiation from colliding black holes in the close limit. *Phys. Rev.*, D65:084034, 2002.

[45] Liebrecht R. Venter and Nigel T. Bishop. Numerical validation of the Kerr metric in Bondi-Sachs form. *Phys. Rev.*, D73:084023, 2006.

[46] S J Fletcher and A W C Lun. The Kerr spacetime in generalized Bondi-Sachs coordinates. *Class. Quant. Grav.*, 20:4153–4167, 2003.

[47] Shan Bai et al. Light cone structure near null infinity of the Kerr metric. *Phys. Rev.*, D75:044003, 2007.

[48] Frans Pretorius and Werner Israel. Quasi-Spherical Light Cones of the Kerr Geometry. *Class. Quant. Grav.*, 15:2289–2301, 1998.

[49] Ernst Nils Dorband, Emanuele Berti, Peter Diener, Erik Schnetter, and Manuel Tiglio. A numerical study of the quasi-normal mode excitation of Kerr black holes. *Phys. Rev.*, D74:084028, 2006.

[50] W. Krivan, P. Laguna, Philippos Papadopoulos, and N. Andersson. Dynamics of perturbations of rotating black holes. *Phys. Rev. D*, 56:3395–3404, 1997.

[51] Lior M. Burko and Gaurav Khanna. Late-time Kerr tails revisited. *Class. Quant. Grav.*, 26:015014, 2009.

[52] Reinaldo J. Gleiser, Richard H. Price, and Jorge Pullin. Late time tails in the Kerr spacetime. *Class. Quant. Grav.*, 25:072001, 2008.

[53] Manuel Tiglio, Lawrence E. Kidder, and Saul A. Teukolsky. High accuracy simulations of Kerr tails: coordinate dependence and higher multipoles. *Class. Quant. Grav.*, 25:105022, 2008.

[54] Shahar Hod. Mode-coupling in rotating gravitational collapse of a scalar field. *Phys. Rev.*, D61:024033, 2000.

[55] R. Penrose. Conformal treatment of infinity. In C.M. DeWitt and B.S. DeWitt, editors, *Relativity, Groups and Topology.*, pages 565–584, New York, U.S.A., 1964. Gordon and Breach.

[56] Robert Geroch. Asymptotic structure of space-time. In F.P. Esposito and L. Witten, editors, *Asymptotic Structure of Space-Time*, pages 1–105. Plenum Press, 1977.

[57] R. M. Wald. *General Relativity*. The University of Chicago Press, Chicago, 1984.

[58] Helmut Friedrich and Alan D. Rendall. The Cauchy problem for the Einstein equations. *Lect. Notes Phys.*, 540:127–224, 2000.

[59] Anıl Zenginoğlu. A conformal approach to numerical calculations of asymptotically flat spacetimes. 2007.

[60] Bengt Fornberg. *A Practical Guide to Pseudospectral Methods*. Cambridge University Press, 1999.

[61] Heinz-Otto Kreiss and Joseph Oliger. Methods for the approximate solution of time dependent problems. *Global atmospheric research programme publications series*, 10, 1973.

[62] E.W. Leaver. An analytic representation for the quasi-normal modes of Kerr black holes. *Proc. R. Soc. London, Ser. A*, 402:285–298, 1985.

[63] E. W. Leaver. An analytic representation for the quasi-normal modes of Kerr black holes. *Proc. R. Soc. London, Series A*, 402(1823):285–298, December 9 1986.

[64] Michael Purrer, Sascha Husa, and Peter C. Aichelburg. News from critical collapse: Bondi mass, tails and quasinormal modes. *Phys. Rev.*, D71:104005, 2005.

[65] Jorg Frauendiener. Numerical treatment of the hyperboloidal initial value problem for the vacuum Einstein equations. III. On the determination of radiation. *Class. Quant. Grav.*, 17:373–387, 2000.

[66] Shahar Hod. The radiative tail of realistic gravitational collapse. *Phys. Rev. Lett.*, 84:10–13, 2000.

[67] Shahar Hod. Mode-coupling in rotating gravitational collapse: Gravitational and electromagnetic perturbations. *Physical Review D*, 61:064018, 2000.

[68] Edward Malec and Niall O Murchadha. Constant mean curvature slices in the extended Schwarzschild solution and collapse of the lapse: Part I. *Phys. Rev.*, D68:124019, 2003.

[69] Edward Malec and Niall O'Murchadha. The general spherically symmetric constant mean curvature foliations of the

Schwarzschild solution. 2009.

[70] Frank Ohme, Mark Hannam, Sascha Husa, and Niall O Murchadha. Stationary hyperboloidal slicings with evolved gauge conditions. 2009.

[71] We use the naming convention for the coordinatization of Kerr spacetime as in [51].